The current issue and full text archieve of this journal is available at
http://www.emeraldinsight.com/0961-5539.htm

Determination of ϵ at inlet boundaries

Bart Merci, Erik Dick, Jan Vierendeels and Chris De Langhe
Ghent University, Department of Flow, Heat and Combustion Mechanics, Gent, Belgium

Received July 2001
Revised October 2001
Accepted October 2001

Keywords *Boundary conditions, Numerical dissipation*

Abstract *Different methods for the determination of accurate values for the dissipation rate ϵ at the inlet boundary of a computational domain, are studied. With DNS data for a fully developed channel flow and pipe flow, it is shown that the method suggested by Rhee and Sung (2000), in which the $k-\epsilon$ turbulence model is used to compute both k and ϵ from a given velocity profile, is not reliable and can result in very poor results. The method is found to be extremely sensitive to the details of the imposed velocity profile. An alternative procedure is proposed, in which only the ϵ transport equation is employed, with given profiles for the mean velocity and the turbulence kinetic energy. This way, accurate and reliable profiles are obtained for ϵ. Another procedure, based on the turbulent mixing length, was suggested by Jones (1994). The problem. The problem is then shifted towards the determination of the mixing length at the inlet boundary of the computational domain. An expression for this mixing length is proposed in this paper, based on the mentioned DNS data. Finally, the method proposed by Rodi and Scheuerer (1985) is included for comparison reasons. The different procedures are first validated on the fully developed channel and pipe flow. Next, the turbulent flow over a backward-facing step is considered. Finally, the influence of the inlet boundary condition for ϵ is illustrated in the application of a turbulent piloted jet diffusion flame.*

1 Introduction

It is obvious that, in a numerical flow calculation, a complete set of boundary conditions is needed at the inlet(s) of the computational domain. In the case of turbulent flow calculations, using standard turbulence models including a modelled equation for the turbulence dissipation rate ϵ, an inlet boundary condition for this quantity is needed. In the literature, the method used to specify this boundary condition often is not described, making it difficult to judge model performance. In this article, predictions of different proposed boundary conditions for the dissipation rate are compared and evaluated, and recommendations are made.

If a test case has been studied by DNS, all the required quantities are readily available and can be correctly imposed as inlet boundary conditions. If, on the other hand, the test case has been studied experimentally, this is no longer true. In many cases, experimental data are available for the mean velocity field and

The first author works as a Postdoctural Fellow of the Fund for Scientific Research—Flanders (Belgium) (F.W.O.-Vlaanderen). The authors wish to thank D. Roekaerts (Delft University of Technology, Department of Applied Physics, The Netherlands) and T.W.J. Peters (Corus Research and Development, The Netherlands) for their help with the reacting test case.

International Journal of Numerical Methods for Heat & Fluid Flow, Vol. 12 No. 1, 2002, pp. 65–80.

DOI 10.1108/09615530210413172

the fluctuations of (one or more) velocity components. From the fluctuations, the inlet profile for the turbulence kinetic energy can be constructed. For a two-equation Reynolds-averaged Navier-Stokes (RANS) turbulence model, an inlet profile for the second turbulence quantity (e.g. the dissipation rate ϵ, is required too. This cannot be readily provided by the experimentalists. In this paper, different procedures to determine ϵ are compared, and a reliable method is proposed.

One possible procedure was described by Rhee and Sung (2000): the $k-\epsilon$ turbulence model is used to determine both k and ϵ from a given velocity profile. It will be illustrated that this method is not reliable: the results are extremely sensitive to the detail of the velocity profile. Therefore, an alternative method is developed in this paper. The profile for ϵ is derived from (experimental) data for the mean velocity and the turbulence kinetic energy k. This procedure will be shown to be far more reliable, since it is less sensitive to the details of the imposed profiles. Another method was suggested by Jones (1994). It is based on the knowledge of the turbulent mixing length. The problem is thus shifted towards the determination of the mixing length. An appropriate expression is proposed in this paper, based on DNS data for a fully developed channel (Kim *et al.*, 1987) and pipe (Eggels *et al.*, 1994) flow. Finally, the method proposed by Rodi and Scheuerer (1985) is included, too, for comparison reasons.

The different procedures are first validated on the fully developed channel and pipe flow. Next, the influence of the inlet boundary conditions for ϵ is described for the turbulent flow over a backward-facing step (Le *et al.*, 1997) and for a turbulent piloted jet diffusion flame (Barlow and Frank, 1998). The low-Reynolds version by Yang and Shih (1993) of the standard $k-\epsilon$ model is used. While the global results are strongly influenced by the choice of the turbulence model, the suggested method for the determination of ϵ at the inlet is illustrated to yield good inlet profiles, particularly for the last test case.

2 Governing equations

The steady state RANS equations are:

$$\begin{cases} \dfrac{\partial}{\partial x_i}(\rho v_i) = 0 \\ \dfrac{\partial}{\partial x_j}(\rho v_i v_j) + \dfrac{\partial p}{\partial x_i} = \dfrac{\partial}{\partial x_j}(\tau_{ij} + \tau_{ij}^T) + \rho f_i, \qquad i = 1, \ldots, d \end{cases} \tag{1}$$

In (1), ρ is the density, v_i is the velocity component in i-direction, p is the pressure, f is an external force and d is the number of dimensions. All averaging symbols are omitted. The molecular and turbulent stress tensors are:

$$\tau_{ij} = 2\mu S_{ij}, \qquad \tau_{ij}^T = 2\mu_t S_{ij} - \tfrac{2}{3}\rho k \delta_{ij}, \tag{2}$$

with μ the dynamic viscosity, k the turbulence kinetic energy and δ_{ij} the Kronecker delta. In (2), the strain rate tensor $\mathbf{S}$ is defined as:

$$S_{ij} = \frac{1}{2}\left(\frac{\partial v_i}{\partial x_j} + \frac{\partial v_j}{\partial x_i}\right) - \frac{1}{3}\delta_{ij}\frac{\partial v_k}{\partial x_k}. \tag{3}$$

The turbulent viscosity is defined as (Yang and Shih, 1993:

$$\mu_t = \rho c_\mu f_\mu k \tau_t, \tag{4}$$

with $c_\mu = 0.09$,

$$f_\mu = [1 - \exp(-1.510^4 R_y - 5.010^{-7} R_y^3 - 1.10^{-10} R_y^5)]^{\frac{1}{2}}$$

(with

$$R_y = \frac{\rho\sqrt{ky}}{\mu}$$

and y the normal distance from the nearest solid boundary), and:

$$\tau_t = \frac{k}{\varepsilon} + \sqrt{\frac{\mu}{\rho\varepsilon}}.$$

The turbulence quantities are determined from the transport equations:

$$\begin{cases} \dfrac{\partial}{\partial x_j}(\rho k v_j) = P_k - \rho\varepsilon + \dfrac{\partial}{\partial x_j}\left[\left(\mu + \dfrac{\mu_t}{\sigma_k}\right)\dfrac{\partial k}{\partial x_j}\right] \\ \dfrac{\partial}{\partial x_j}(\rho\varepsilon v_j) = (c_{\varepsilon 1} P_k - c_{\varepsilon 2} f_2 \rho\varepsilon)\dfrac{1}{\tau_t} + \dfrac{\partial}{\partial x_j}\left[\left(\mu + \dfrac{\mu_t}{\sigma_\varepsilon}\right)\dfrac{\partial \varepsilon}{\partial x_j}\right] + E, \end{cases} \tag{5}$$

with:

$$P_k = \tau_{ij}^T \frac{\partial v_j}{\partial x_i}.$$

The model constants are $\sigma_k = 1$, $\sigma_\epsilon = 1.3$, $c_{\epsilon 1} = 1.44$ and $c_{\epsilon 2} = 1.92$. The damping function f_2 is:

$$f_2 = 1 - 0.22\exp\left(-\frac{\mathrm{Re}_t^2}{36}\right).$$

The low-Reynolds source term is:

$$E = \frac{\mu}{\rho}\mu_t \frac{\partial^2 v_i}{\partial x_j \partial x_k}\frac{\partial^2 v_i}{\partial x_j \partial x_k}.$$

For completeness, it is mentioned that at solid boundaries $k_w = 0$ and ϵ_w is determined from:

$$\varepsilon_w = 2\frac{\mu}{\rho}\left(\frac{\partial\sqrt{k}}{\partial y}\right)^2. \tag{6}$$

3 Determination of ϵ

3.1 Rhee and Sung's method (Rhee and Sung, 2000)

In this procedure, both k and ϵ at the inlet boundary are determined from a separate calculation. They are computed in the inlet plane from equation (5), under the assumption of fully developed flow conditions, with an imposed velocity profile:

$$\begin{cases} 0 = P_k - \rho\varepsilon + \dfrac{\partial}{\partial x_j}\left[\left(\mu + \dfrac{\mu_t}{\sigma_k}\right)\right]\dfrac{\partial k}{\partial x_j} \\ 0 = (c_{\varepsilon 1}P_k - c_{\varepsilon 2}f_2\rho\varepsilon)\dfrac{1}{\tau_t} + \dfrac{\partial}{\partial x_j}\left[\left(\mu + \dfrac{\mu_t}{\sigma_\varepsilon}\right)\dfrac{\partial\varepsilon}{\partial x_j}\right] + E. \end{cases} \tag{7}$$

The velocity profile, introduced into P_k and E in (7), is obtained from experimental data.

The expression of fully developed flow conditions ensures that the profiles imposed at the inlet, remain unchanged downstream (as long as the flow is not influenced by its environment). However, the system of transport equations (7), is ill-conditioned: since $c_{\epsilon 1}$ and $c_{\epsilon 2}$ do not differ much, and the viscous terms and the near-wall term are typically small in the bulk flow, the two equations become practically identical, so that the system tends to be nearly singular. As a consequence, the resulting profiles for k and ϵ are very sensitive to the detail of the imposed velocity profile, which makes the method unattractive. This is illustrated in Figures 1 and 2, showing profiles for a turbulent fully developed channel flow, for which DNS data are available (Kim *et al.*, 1987). When the imposed velocity profile is taken from the DNS data, curves 1 result for k and ϵ. If, on the other hand, the mean velocity is computed from equation (1) curves 2 result. Figure 1 (left) illustrates that the differences between the DNS and the computed velocity profiles are extremely small (the Yang-Shih model has been calibrated for this flow). Still, the profiles for k and ϵ are considerably different. This illustrates that the resulting profiles are extremely sensitive to details in the imposed vehicle profile, as already explained. Moreover, it is seen that the profiles for k and ϵ are better when the computed velocity profile is used, instead of the DNS profile. This illustrates that the $k-\epsilon$ model is not suited for the calculation of k and ϵ simultaneously, with an imposed velocity profile. When the complete set of equations (1) and (5) is solved, the velocity profile is

allowed to undergo small variations from the DNS profile, and more realistic profiles for both k and ϵ result. To conclude, it is noted that the deviations are indeed mostly pronounced in the bulk flow, where both k and ϵ are seriously overestimated.

3.2 Proposed method

Considering the sensitivity of the previous method to the details of the imposed velocity profile, due to the ill-conditioned system (7), an alternative method is suggested. In many experiments, both the mean velocities and velocity fluctuations are measured at the inlet. When the fluctuations are known for all three velocity components, the turbulence kinetic energy is readily determined as:

$$k = \tfrac{1}{2} v'_i v'_{\dot{\tau}}$$

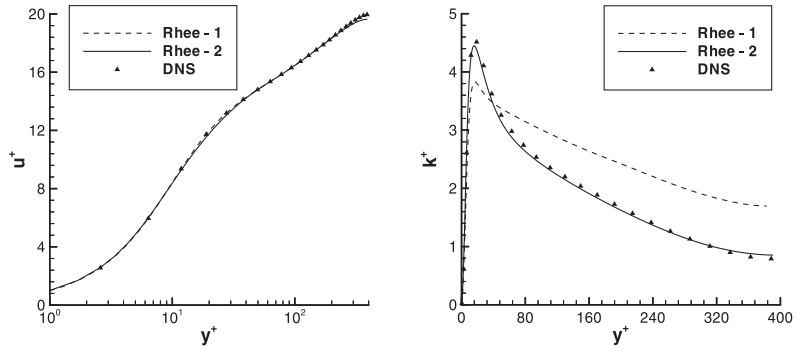

Note: 1: velocity from DNS; 2: velocity calculated from eqs. (1)

Figure 1.
Influence of the imposed mean velocity profile (left) on the computed turbulence kinetic energy (right) in Rhee and Sung's method for the fully developed channel flow

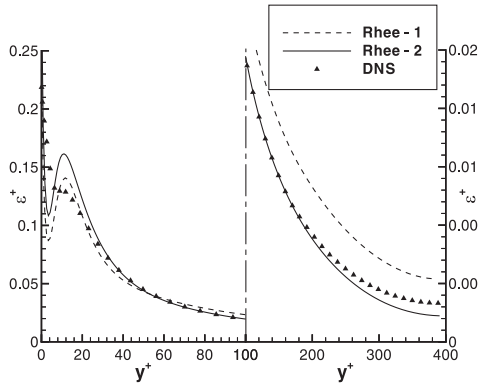

Note: scale break at $y^+ = 100$. (1,2: see fig. 1)

Figure 2.
Influence of the imposed mean velocity profile on the computed ϵ in Rhee and Sung's method for the fully developed channel flow

(with the summation convention). Often, fluctuations are measured for only one or two velocity components. If both $\overline{u'u'}$ and $\overline{v'v'}$ have been measured, the approximation $\overline{w'w'} = \overline{v'v'}$ is applied to determine k. This is justified, since in general these fluctuations do not differ much, and they are smaller than $\overline{u'u'}$, as illustrated by DNS data for the channel (Kim *et al.*, 1987) and pipe (Eggels *et al.*, 1994) flow. If only $\overline{u'u'}$ is known, a reasonable approximation is:

$$\overline{w'w'} = \overline{v'v'} = \tfrac{1}{2}\overline{u'u'},$$

again based on the mentioned DNS data.

Once the profiles for the mean velocity and the turbulence kinetic energy are known, the ϵ-profile is determined, under the assumption of fully developed conditions from:

$$0 = (c_{\varepsilon 1} P_k - c_{\varepsilon 2} f_2 \rho \varepsilon) \frac{1}{\tau_t} + \frac{\partial}{\partial x_j}\left[\left(\mu + \frac{\mu_t}{\sigma_\varepsilon}\right)\frac{\partial \varepsilon}{\partial x_j}\right] + E. \tag{8}$$

Again, the expression of fully developed flow conditions ensures that the inlet profiles remain unchanged downstream. It is noteworthy that when the measured profiles of mean velocity and/or velocity fluctuations do not correspond to completely fully developed flow conditions, the described method remains valid. Since only the ϵ-equation (equation 8) is solved, rather than the (ill-conditioned) system (7), the method is much less sensitive to the details of the imposed profiles of both mean velocity and turbulence kinetic energy. This will be discussed further in Section 4.1. Finally, it is noted that a separate calculation for the inlet profile of ϵ remains necessary, as in Rhee and Sung's method (Rhee and Sung, 2000). However, the computational grid for the calculation of the inlet ϵ profile, consists of only one line for two-dimensional or axisymmetric calculations, so that the additional computing times are very short.

3.3 Jones' method (Jones, 1994)

An alternative method, commonly used for reacting flow calculations, is the determination of ϵ from a mixing length (Jones, 1994):

$$\varepsilon = \frac{c_\mu^{3/4} k^{3/2}}{l_m}, \tag{9}$$

where $c_\mu = 0.09$ and l_m is the Prandtl mixing length. The problem has now been shifted towards the determination of the mixing length. Jones (1994) suggests to use the relation $l_m = \kappa y$, in correspondence with a well-known expression, valid for the turbulent flow over a flat plate, due to Van Driest:

$$l_m = \kappa y(1 - \exp(-y^+/26)), \tag{10}$$

where $\kappa = 0.4$ is the von Karman constant and $y^+ = \rho y u_\tau / \mu$, with y the distance from the nearest solid boundary and $u_\tau = \sqrt{\tau_w/\rho}$ the friction velocity.

Using the DNS databases for the fully developed channel (Kim *et al.*, 1987) and pipe (Eggels *et al.*, 1994) flows, an expression for the mixing length can be derived from (9) for these flows, by introducing the DNS values for k and ϵ. The resulting profiles for l_m/y and l_m/H (with H the total height of the channel) or l_m/D (with D the pipe diameter) are shown on the left side of Figure 3 (symbols). For the channel flow, profiles are shown for two different Reynolds numbers $\mathrm{Re} = U_m H/\nu = 6500$ and $\mathrm{Re} = 15800$. For the pipe flow, the Reynolds number is $\mathrm{Re} = U_m D/\nu = 5300$. It is clearly seen that the profiles for l_m/H (or l_m/D) have a much more smooth behaviour than l_m/y. Therefore, curve fitting has been applied for l_m/H (or l_m/D). Further, the behaviour is very similar for the channel flows and the pipe flow. The only difference seems to be due to the Reynolds number, which is in fact low for all three flows. The mixing length at the symmetry axis increases with increasing Reynolds number. For high Reynolds number pipe flows (up to $\mathrm{Re} = 10^6$), Nikuradse proposed the following expression (Schlichting, 1979): $l_m/R = 0.14 - 0.08(1 - y/R)^2 - 0.06(1 - y/R)^4$, with $R = D/2$. Thus, $l_m/D = 0.07$ seems to be an upper limit for l_m at the axis for high Reynolds number flows. As a final consideration for the curve fitting, the limiting behaviour at a solid boundary ($y \to 0$) is studied. Since $l_m \sim k^{3/2}/\epsilon$ (Eq. (9)), and $k \sim y^2$ and ϵ becomes a finite number when $y \to 0$, the mixing length must be $l_m \sim y^3$ for $y \to 0$. To conclude, the result of the curve fitting is:

$$\frac{l_m}{H/D} = \left(1 - \exp\left(-210^6\left(\frac{y}{H/D}\right)^3\right)\right)\left(\frac{1}{15} - \left(\frac{1}{2} - \frac{y}{H/D}\right)^4\right). \qquad (11)$$

The first factor ensures the correct limiting behaviour for $y \to 0$. The factor 1/15 is close to the limit $l_m/D = 0.07$, and the last term is similar to the last term in Nikuradse's expression. So, the expression is meant to be valid for higher

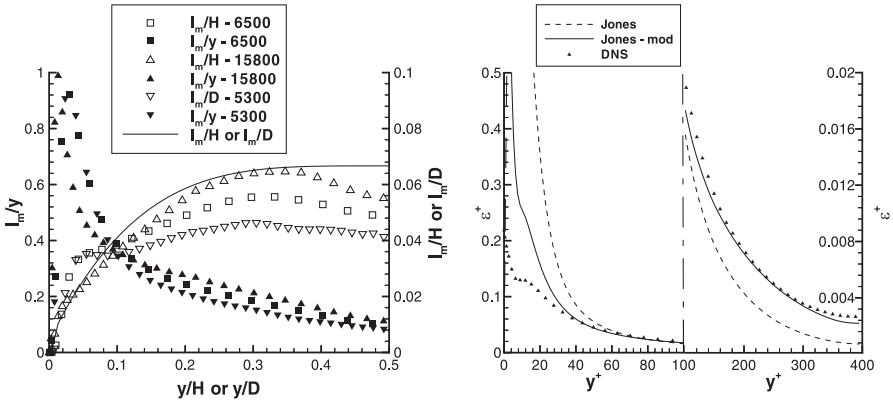

Figure 3.
Left: mixing length from Eq. (9) form DNS data (symbols) and curve fitting (Eq. (11)) (line). Right: profiles for ϵ from Eq. (9) with Eq. (10) ("Jones") and (11) ("Jones—mod") for the fully developed channel flow.

Reynolds number flows. For more complex configurations (e.g. the flow through two concentric cylinders), the diameter D must be replaced by the hydraulic diameter D_h. In the results, the combination (9) with (11) will be denoted "modified Jones".

The result of the curve fitting is depicted by the line in Figure 3 (left). On the right part of the figure, the ϵ profiles are shown for the channel flow, as calculated from the DNS data for k with equation (9), with expression (10) (dashed line) and (11) (solid line). It is clear that the profile from (11) is much better in the bulk flow. Indeed, in the left part of Figure 3, it is seen that $l_m/y \approx 0.15$ in the bulk flow. This value is much smaller than the value 0.4, as suggested by (10). Consequently, ϵ is seriously underestimated when (10) is used. Furthermore, the value for ϵ at the wall is zero with (10), in contrast to the DNS data. On the other hand, the use of (11) may lead to serious overpredictions for ϵ in the neighbourhood of solid boundaries, as illustrated in Figure 3 (right). This, too, is seen in the left part of Figure 3: the mixing length can be strongly underestimated close to the wall, so that ϵ is overestimated. A simple adjustment can be made, though: ϵ can be limited to $\epsilon < \epsilon_w$ (with ϵ_w determined from (6)), so that strong overpredictions are avoided. The main advantage of this method is that no separate calculations are required for the determination of the inlet profiles.

3.4 Rodi and Sheuerer's method (Rodi and Scheuerer, 1985)

Finally, the method by Rodi and Scheuerer (1985) is tested, too:

$$\varepsilon = 0.1k\left|\frac{\partial u}{\partial y}\right|. \tag{12}$$

Thanks to its simplicity, this procedure is useful when the results are not critically dependent on the inlet boundary conditions, as is e.g. the case in the original application (Rodi and Scheuerer, 1985). It is also used sometimes for calculations of the turbulent flow over a flat plate. It is immediately seen, though, that $\epsilon = 0$ is the result at solid boundaries (since $k = 0$), in contrast to DNS data. Also at symmetry axes, where

$$\frac{\partial u}{\partial y} = 0,$$

the unphysical result $\epsilon = 0$ is obtained.

4 Results

4.1 Channel flow

This test case has been studied by DNS (Kim *et al.*, 1987). The ϵ profiles obtained from the different methods described in Section 3, are shown in Figure 4. For Rhee and Sung's and the newly proposed method, the computational grid

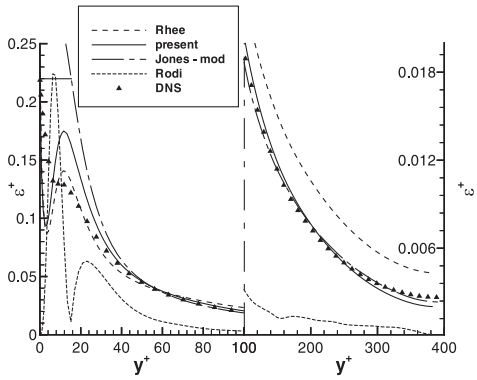

Note: scale break at $y^+ = 100$. ('Jones - mod': see fig. 3)

Figure 4.
Profiles for ϵ for the fully developed channel flow

consists of 1×129 points. The results on a refined grid (1×257 points) coincide, proving their grid independence.

The profiles are dimensionless:

$$\varepsilon^+ = \frac{\varepsilon \mu}{\rho \mu_\tau^4}$$

as a function of

$$y^+ = \frac{y u_\tau \rho}{\mu}.$$

The curve obtained from Rhee and Sung's method (with imposed velocity profile from the DNS data) gives good results close to the wall, but yields a serious overprediction of ϵ in the bulk flow. As explained in Section 3.1, it is indeed in that region that system (7) tends to be nearly singular. The profile obtained from the procedure proposed in Section 3.2 is accurate throughout the channel. The profile is also hardly influenced by the details of the imposed profiles for mean velocity and turbulence kinetic energy. This can be seen from a comparison with curve 2 from Figure 2, which would be obtained with the proposed procedure if the computed profiles for velocity and turbulence kinetic energy were imposed instead of the DNS profiles. This reveals that there is hardly any difference. The ϵ profile obtained from (9), with (11), gives good results in the bulk flow, but has a poor behaviour close to the wall. However, as illustrated in Figure 4, applying the cut-off $\epsilon < \epsilon_w$ (with ϵ_w from (6)) resolves the problem. The result from (12) is very poor. As mentioned, both at the wall ($k = 0$) and at the symmetry axis

$$\left(\frac{\partial u}{\partial y} = 0 \right),$$

$\epsilon = 0$ is obtained, in contrast to the DNS data. Globally, ϵ is seriously underpredicted.

4.2 Pipe flow

This test case has also been studied by DNS (Eggels *et al.*, 1994). The different ϵ profiles are shown in Figure 5. for Rhee and Sung's and the newly proposed method, the computational grid consists of 1×129 points. The results on a refined grid (1×257 points) coincide, proving their grid independence.

The profiles are dimensionless:

$$\varepsilon^+ = \frac{\varepsilon D}{\mu_\tau^3}$$

as a function of

$$y^+ = \frac{y u_\tau \rho}{\mu}.$$

Again, Rhee and Sung's method results in an overprediction for ϵ in the bulk flow when the imposed velocity profile is taken from the DNS data. Also close to the wall, ϵ is overpredicted now. The procedure proposed in Section 3.2 yields accurate results, as does the method from Section 3.3, with (11) used in (9). Again the cut-off $\epsilon < \epsilon_w$ can resolve the overprediction near the wall. As for the channel flow, Rodi and Scheuerer's method gives poor results.

The sensitivity of Rhee and Sung's method to the detail of the imposed velocity profile is illustrated once more in Figure 6. Again, imposing the DNS velocity profile (curves 1) yields worse results than using the computed velocity profile (curves 2). Note that the method proposed in Section 3.2 is again less sensitive to details in the velocity profiles. This is seen from a comparison of curve "present" from Figure 5 to curve 2 from Figure 6, which would be obtained with the proposed procedure if the computed profiles for velocity and

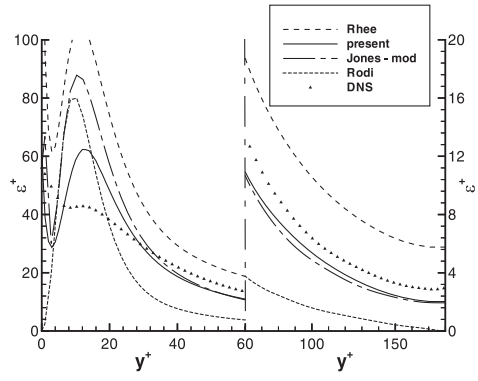

Note: scale break at $y^+ = 60$. ('Jones - mod': see fig. 3)

Figure 5.
Profiles for ϵ for the fully developed pipe flow

turbulence kinetic energy were imposed instead of the DNS profiles. The difference is not negligible for this test case, due to the larger differences between the computed and the DNS velocity profiles.

4.3 Backward-facing step

This test case has also been studied by DNS (Le *et al.*, 1997). The computational grid consists of 129 × 145 grid points. The domain starts three step heights H ahead of the step (because DNS profiles are available for that position) and extends to 20 H downstream. The height of the domain is 6 H. Since the inlet of the computational domain is not located at the step, the influence of the inlet profiles on the results is reduced. Consequently, although this test case is used by Rhee and Sung (2000), it is in fact not suitable for the judgement of the quality of the inlet profiles. Still, some tendencies can be recognised in the details of the results, as will be discussed next.

The left part of Figure 7 shows the evolution of the friction coefficient:

$$c_f = \frac{\tau_w}{\frac{1}{2}\rho u_0^2}, \tag{13}$$

with τ_w the shear stress at the wall and u_0 the free stream velocity. The result is of course determined by the choice of the turbulence model. Still, comparison of the different profiles reveal the influence of the inlet ϵ profiles.

First of all, it is observed that the recirculation length (where c_f = 0) is underpredicted due to an overprediction of k (and μ_t) by the $k-\epsilon$ model in the recirculation zone. The overprediction of c_f downstream is a consequence of the overpredictions of k, too (Merci, 2000; Merci *et al.*, 2001a). From the different c_f profiles, it is seen that all curves correspond well. This illustrates that the influence of the inlet ϵ profile is not substantial for this test case. However, when Rhee and Sung's method is applied for the inlet profiles, c_f is more strongly overpredicted in the downstream region. Indeed, as was the case for

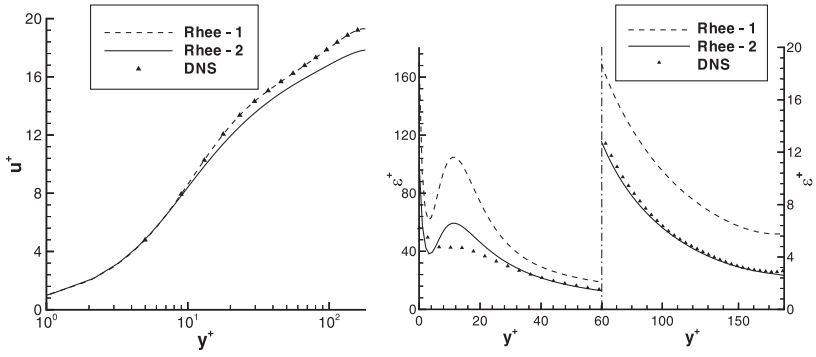

Figure 6.
Influence of the imposed mean velocity profile (left) on the computed ϵ (right) in Rhee and Sung's method for the fully developed pipe flow. (1, 2: see Figure 1)

the channel flow (Figure 1), the turbulence kinetic energy is overpredicted in the free stream at the inlet (not shown). This is illustrated in the right part of Figure 7, showing the profile of k/u_0^2 at $x/H = 4$, which is situated in the recirculation region. In the region $y/H > 1{,}5$, higher values of k are observed for the "Rhee" curve. Close to the wall, the differences with the "present" curve are negligible, which explains the very similar c_f profiles in the recirculation region. The reasons for this are that the differences between the inlet profiles are relatively small near the solid boundary (as in Figures 1 (right) and 4) and that the value for k in the recirculation region is more determined by the flow processes in that region than by the inlet values. Still, as is seen from the overprediction of c_f by Rhee and Sung's method downstream, due to the overprediction of k at the inlet, the influence of the inlet profiles is seen in the global results, and the procedure proposed in Section 3.2 yields more accurate results.

When the inlet profile is determined from (9) with (10), very similar results are obtained as with the method proposed in Section 3.2. This illustrates once again that the test case is not sensitive with respect to the inlet profiles. Note that expression (10) is used, since the incoming flow is free, so that no channel height can be defined for (11). Moreover, it is known that (10) yields good results for the flow over a flat plate.

Finally, it is seen that Rodi and Sheuerer's method also yields similar results, again thanks to the lack of sensitivity on the inlet profiles. Still, the global underprediction of k (Figure 7, right) and thus a slightly shorter recirculation length and higher values for c_f downstream (Figure 7, left).

For completeness, it is mentioned that calculations have also been performed on a refined grid (257×289 points). The results are grid independent (not shown).

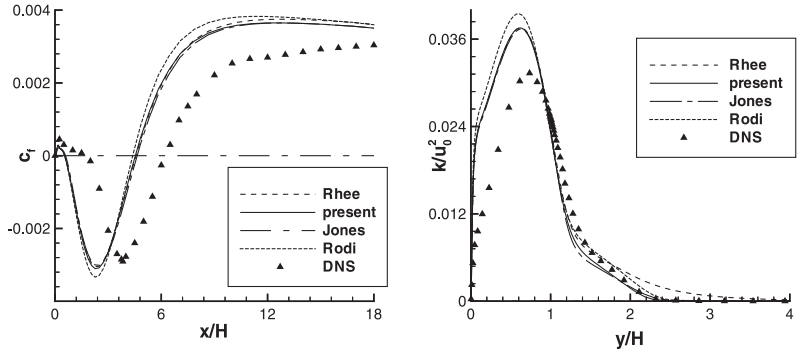

Figure 7.
Left: friction coefficient for the turbulent flow over a backward-facing step. Right: turbulence kinetic energy at $x/H = 4$

The conclusion of this test case is that, even though the results are insensitive to the inlet profiles, their influence is still noticeable. Exactly the same tendencies were found as for the channel flow.

4.4 Piloted jet diffusion flame

This test case has been studied experimentally (Barlow and Frank, 1998; Schneider, 2000). A central fuel jet mixes with a co-flow air stream). In between, a pilot stream is supplied, ensuring a stable flame. The Burke-Schumann flame sheet model is used as chemistry model, in combination with a pre-assumed β-PDF approach. Radiation has been neglected. These choices have little influence on the flow field predictions (Merci, 2000; Merci *et al.*, 2001b)

In order to account for variable density effects, a term is added in the right-hand-side of the k and ϵ transport equation (5):

$$\begin{cases} \dfrac{\partial}{\partial x_j}(\rho k v_j) = P_k - \rho\varepsilon + \dfrac{\partial}{\partial x_j}\left[\left(\mu + \dfrac{\mu_t}{\sigma_k}\right)\dfrac{\partial k}{\partial x_j}\right] - \dfrac{\mu_t}{\rho}\dfrac{\partial \rho}{\partial x_i}\dfrac{\partial p}{\partial x_i} \\ \dfrac{\partial}{\partial x_j}(\rho\varepsilon v_j) = \left(c_{\varepsilon 1}P_k - c_{\varepsilon 2}f_2\rho\varepsilon - \dfrac{\mu_t}{\rho}\dfrac{\partial \rho}{\partial x_i}\dfrac{\partial p}{\partial x_i}\right)\dfrac{1}{\tau_t} + \dfrac{\partial}{\partial x_j}\left[\left(\mu + \dfrac{\mu_t}{\sigma_\varepsilon}\right)\dfrac{\partial \varepsilon}{\partial x_j}\right] + E. \end{cases} \tag{14}$$

The extra terms are small for the test case under study (Merci, 2000; Merci *et al.*, 2001b). The transport equations for the mean mixture fraction ξ and its variance g are (Merci *et al.*, 2001b):

$$\begin{cases} \dfrac{\partial}{\partial x_j}(\rho\xi v_j) = \dfrac{\partial}{\partial x_j}\left[\left(D + \dfrac{\mu_t}{\sigma_\xi}\right)\dfrac{\partial \xi}{\partial x_j}\right] \\ \dfrac{\partial}{\partial x_j}(\rho g v_j) = \dfrac{\partial}{\partial x_j}\left[\left(\mu + \dfrac{\mu_t}{\sigma_g}\right)\dfrac{\partial g}{\partial x_j}\right] + 2\dfrac{\mu_t}{\sigma_\xi}\dfrac{\partial \xi}{\partial x_i}\dfrac{\partial \xi}{\partial x_i} - c_g\rho g\dfrac{1}{\tau_t}, \end{cases} \tag{15}$$

with D the molecular diffusivity. The model constants are $\sigma_\xi = 0.7$, $\sigma_g = 0.7$ and $c_g = 2$.

The computational grid contains 81×89 points. The inlet boundary coincides with the nozzle exit. As a consequence, the results are very sensitive to the inlet profiles. Experimental data are available for the mean velocity and its fluctuations at the inlet. Both axial and radial fluctuations have been measured (Schneider, 2000), from which k is constructed with the assumption $w'w' = v'v'$. No data are available for ϵ, so that the quality of the inlet ϵ profile can only be judged indirectly. To that purpose, the axial velocity profile is shown on the symmetry axis in Figure 8. The profile has been made dimensionless through division by the velocity on the axis at the nozzle exit. The axial coordinate is divided by the nozzle diameter.

For the application of Rhee and Sung's method, only the measured velocity profiles are imposed, while both k and ϵ are computed. As a consequence, k is actually overpredicted (not shown). The result is that the velocity decays too steeply close to the nozzle exit ($x/D_n < 20$), due to an overprediction of the turbulent shear stress (not shown). Applying the procedure proposed in Section 3.2, with k determined from the measurements as described above, completely resolves the problem, as illustrated in Figure 8. Finally, when ϵ is determined from (9) with (11), reasonable results are achieved, too. There seems to be a slight underprediction of ϵ, resulting in an overprediction of the turbulent shear stress and thus a slightly too steep velocity decay near the nozzle exit. It is noteworthy that the use of (10) yields worse results (not shown), since then on the axis the mixing length is $l_m = 0.2D_n$, instead of $l_m = 0.667D_n$, so that ϵ is more strongly underpredicted. Further downstream, all curves have a similar behaviour, governed by the chosen turbulence model. In any case, it is clear that the inlet conditions for ϵ remain of importance throughout the flow field, and that the method proposed in Section 3.2 ensures good results near the nozzle exit, indicating that the inlet profiles are indeed accurate. Thanks to the good behaviour near the nozzle exit, the results downstream show better agreement with the experimental data.

Finally, it is mentioned that the calculations have also been performed on a refined grid (161 × 177 points). The results coincide (not shown), indicating the grid independence of the results.

5 Conclusions

Different methods to determine the dissipation rate at the inlet of a computational domain, have been studied. It has been explained that an

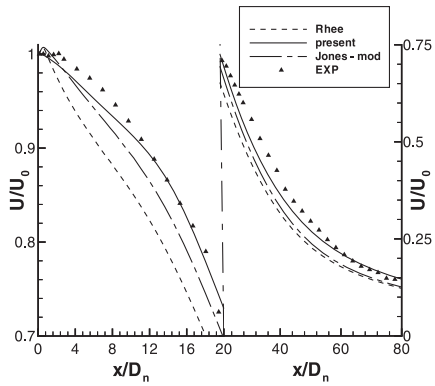

Note: scale break at $x/D_n = 20$. ('Jones - mod': see fig. 3)

Figure 8.
Mean velocity on the axis for the piloted jet diffusion flame

existing method (Rhee and Sung, 2000), in which profiles of both k and ϵ are determined from given velocity profiles in a separate calculation, is very sensitive to the details of these velocity data. As a consequence, this method is not reliable. An alternative procedure has been proposed, in which only ϵ is computed from given velocity and k profiles. This procedure does not suffer from the sensitivity problem.

Alternatively, the inlet profile for ϵ can be determined from the mixing length (Jones, 1994). An appropriate expression for the mixing length as a function of the distance from the nearest solid boundary has been determined on the basis of DNS data for both a channel and a pipe flow. Using this expression, while limiting ϵ to values smaller than the value at the solid boundary, yields reasonable results, too. They are slightly less accurate than the ones from the proposed procedure, though.

The different procedures have been firstly validated on a fully developed channel (Kim *et al.*, 1987) and pipe (Eggels *et al.*, 1994 flow. Next, the turbulent flow over a backward-facing step has been studied. Though this flow is less sensitive to the inlet conditions, their influence was noticeable. Finally, a piloted jet diffusion flame (Barlow and Frank, 1998; Schneider, 2000) has been considered. For this case, the inlet conditions have a substantial influence in the complete computational domain. For all the test cases, the proposed procedure yields the most accurate and reliable results. The mixing length method, in combination with the proposed expression for the mixing length, yields reasonable results, too.

References

Barlow, R.S. and Frank, J.H. (1998), "Effects of turbulence on species mass fractions in methane/air jet flames", in The Combustion Institute (Ed.), *27th Symposium (International) on Combustion*, Pittsburgh, pp. 1087–95. (Data also available on: www.ca.sandia.gov/tdf/workshop.html)

Eggels, J.G.M., Unger, F., Weiss, M.H., Westerweel, J., Adrian, R.J., Friedrich, R. and Nieuwstadt, F.T.M. (1994), "Fully developed turbulent pipe flow: a comparison between direct numerical simulation and experiment", *Journal of Fluid Mechanics*, Vol. 268, pp. 175–209.

Jones, W.P. (1994), "Turbulence modelling and numerical solution methods", in Libby, P.A., Williams, F.A., (Eds) *Turbulent Reacting Flows*, Academic Press, London, pp. 309–74.

Kim, J., Moin, P. and Moser, R. (1987), "Turbulence statistics in fully developed channel flow at low Reynolds number", *Journal of Fluid Mechanics*, Vol. 177, pp. 133–66.

Le, H., Moin, P. and Kim, J. (1997), "Direct numerical simulation of turbulent flow over a backward-facing step", *Journal of Fluid Mechanics*, Vol. 330, pp. 349–74.

Merci, B. (2000), "Numerical simulation and modelling of turbulent combustion", PhD thesis, Ghent University Belgium.

Merci, B., De Langhe, C., Vierendeels, J. and Dick, E. (2001a), "A quasi-realizable cubic low-Reynolds eddy-viscosity turbulence model with a new dissipation rate equation", *Flow, Turbulence and Combustion*, Vol. 66 No. 2, pp. 133–57.

Merci, B., Roekaerts, D., Peeters, T.W.J., Dick, E. and Vierendeels, J. (2001b), "Application of a new cubic turbulence model to piloted and bluff-body diffusion flames", *Combustion and Flame*, Vol. 126 No. 1-2, pp. 1533–56.

Rhee, G.H. and Sung, H.J. (2000), "Generation of inflow conditions in a Reynolds-averaged Navier-Stokes closure", *AIAA Journal*, Vol. 38 No. 3, pp. 545–47.

Rodi, W. and Scheuerer, G. (1985), "Calculation of heat transfer to convection-cooled gas turbine blades", *Journal of Engineering for Gas Turbines and Power*, Vol. 107, pp. 620–37.

Schlichting, H. (1979), *Boundary Layer Theory*, McGraw-Hill Series in Mechanical Engineering, 4th ed., McGraw-Hill, p. 605.

Schneider, C. (2000), private communication.

Yang, Z.Y. and Shih, T.H. (1993), "A new time scale based $k-\epsilon$ model for near-wall turbulence", *AIAA Journal*, Vol. 31 No. 7, pp. 1191–98.